A simulation study on the focal plane detector of the LAUE project

M. Khalil [a,b,*], F. Frontera [b,c], E. Caroli [c], E. Virgilli [b], V. Valsan [b]

[a] APC Laboratory, 10 rue Alice Domon et Léonie Duquet, 75205 Paris Cedex 13, France
[b] Department of Physics and Earth Sciences, University of Ferrara, Via Saragat, 1, 44100 Ferrara, Italy
[c] INAF/IASF-Bologna, Via P. Gobetti 101, Bologna, Italy

A B S T R A C T

The LAUE project, supported by the Italian Space Agency (ASI), is devoted to the development of a long focal length (even 20 m or longer) Laue lens for gamma ray astronomy between 80 and 600 keV. These lenses take advantage of Bragg diffraction to focus radiation onto a small spot drastically improving the signal to noise ratio as well as reducing the required size of the detector significantly. In this paper we present a Monte-Carlo simulation study with MEGALIB to optimize, for space applications, the detector size to achieve high detection efficiency, and to optimize the position resolution of the detector to reconstruct the Point Spread Function of the lens considered for the LAUE project. Then we will show simulations, using the SILVACO semiconductor simulation toolkit, on the optimized detector to estimate its capacitance per channel and depletion voltage. In all of the simulations, two materials were compared; a low density material (Silicon) and a high density material (Germanium).

1. Introduction

Astrophysical observations above 80 keV have been only performed by direct-viewing instruments whose sensitivity is limited by the background. Many astrophysical issues are still open at these energies [1]. For example, the origin of matter–antimatter annihilation emission at 511 keV from the Galactic Center and the accretion physics in Active Galactic Nuclei above 100 keV.

To increase the sensitivity, a new generation of broad band X-ray focusing telescopes that extend the operative energy up to several hundreds of keV is needed. The most efficient technique to focus photons above 80 keV appears to be the Bragg diffraction from bent crystals in a Laue geometry. In general, when photons of energy E impinge on crystals with grazing angle θ_B with respect to a set of atomic planes of Miller index ($h\ k\ l$), they are diffracted according to the Bragg diffraction law:

$$2d_{hkl}\ \sin\ \theta_B = n\frac{hc}{E} \tag{1}$$

The LAUE project [2], supported by the Italian Space Agency (ASI), is a project dedicated to create a technology to construct a Laue lens with a focal length of 20 m able to focus photons in the 80–600 keV energy band. LAUE will be able to perform deep sensitive studies of astrophysical sources. It will, for example, disentangle the source physics, the emission mechanisms at work and discover new physics [3]. A Laue lens focuses gamma rays by using Bragg diffraction in the Laue geometry, i.e. in transmission. A large amount of crystal pieces are arranged in concentric rings and oriented to diffract the X-ray radiation coming from a source at infinity toward a common point (Fig. 1). Each crystal ring is symmetrical with respect to the line of sight of the lens.

Perfect single crystals are not convenient for the construction of a Laue lens given that their response covers a very narrow energy band (corresponding to the Darwin width of the crystal). Mosaic flat crystals were the first attempt to overcome the pass band requirements. In mosaic crystals, thanks to the microcrystals orientation distribution with respect to a main direction, an energy pass band corresponding to 30″–60″ is typically obtained. Bent crystals, instead, are the ideal elements to cover the entire lens surface, by obtaining a continuous (free of gaps) energy pass band.

The lens of our project has a spherical shape with radius R and focal length $f=R/2$, and makes use of bent crystals with curvature radius equal to R. In this configuration the lens becomes a real imaging focusing instrument, as will be discussed elsewhere. In the lens focus a detector is positioned, hereafter called a focal plane detector. The focal plane detector, we assume for space astronomical observations thus a space worthy instrument, is formed of several layers of Double Sided Strip Detectors (DSSDs [4]). Because they are position sensitive, these detectors are able to reconstruct the point spread function (PSF) of a Laue lens, which describes the two dimensional distribution of photons in the focal plane of the lens for a point source at infinity.

* Corresponding author at: APC Laboratory, 10 rue Alice Domon et Léonie Duquet, 75205 Paris Cedex 13, France.
E-mail address: mkhalil@in2p3.fr (M. Khalil).

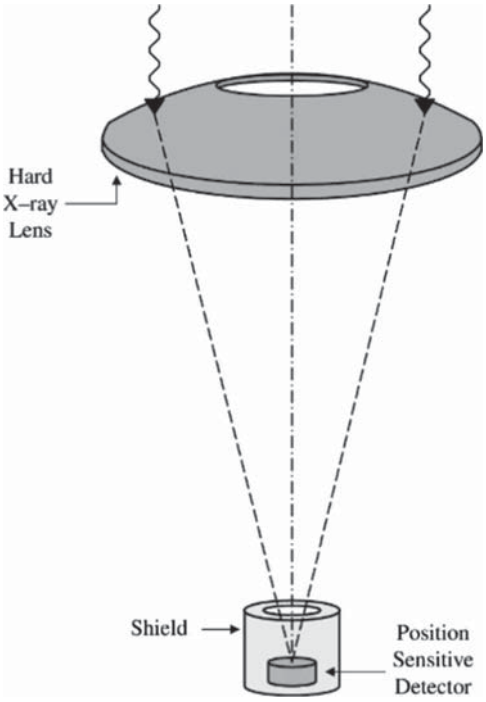

Fig. 1. Pictorial view of a Laue lens (not to scale). The lens is made of mosaic crystal tiles in transmission configuration. The impinging photons are diffracted by the crystal tiles and focused onto a small region centered in the focus of the lens where a position sensitive detector is positioned [5].

Table 1
Parameters of the lens made by GaAs (2 2 0) crystal tiles.

Parameter	Value
Energy range	80–600 keV
Focal length	20 m
No. of rings	45
Minimum radius	20.71 cm
Maximum radius	152.71 cm
Crystal material	GaAs (2 2 0)
Crystal dimension	30 mm × 10 mm × 2 mm

Using MEGALIB [6], we have performed a simulation on the focal plane detector, assumed to be 3D position sensitive. In this study two types of material were compared: a high density material (Germanium) and a low density material (Silicon). The objectives of the simulation were:

- Optimizing the volume of the focal plane detector to achieve a detection efficiency of at least 80% for the 558–645 keV photons (i.e. the photons at the upper threshold of the Lens's pass band).
- Optimizing the 2D position resolution in the focal plane in order to reconstruct the PSF under the condition that the peak intensity profile of the PSF is spread over at least 3 strips.

Hence the main goal of this paper is to optimize the coupling of the Laue lens and the detector in terms of efficiency and 2D spatial resolution. The depth resolution of the detector is not optimized in this work and typical values are assumed for each type of detector material; these will be mentioned in their corresponding sections. In addition, the detector background will be studied and taken into account in future development of the simulation work that will be presented in this paper. Despite this, we will make some considerations on the expected background for each of the considered detector material.

After optimizing the performance of the DSSDs with MEGALIB, the volume and pitch of the detectors were defined. Using the SILVACO [7] semiconductor simulation toolkit, the response of the optimized DSSDs was simulated to obtain the following information:

- The required full depletion voltage.
- The noise of the detector: capacitance and leakage current.

In the following we present the results of this study.

2. Modeling of the lens and the detector in MEGALIB

2.1. LAUE lens modeling

Bent crystals of Ge (1 1 1) and GaAs (2 2 0) with a 2 mm thickness have been selected for the LAUE project, both in transmission configuration. With a uniform thickness, the lens reflection efficency is not optimized, but this choice was imposed by current technological limitations [2]. A detailed study has been performed on these crystals in [8]. Part of this study included the simulation of an entire LAUE lens made of GaAs (2 2 0) crystals that are bent along the Laue lens radius. The lens parameters are given in Table 1. Each of the 45 rings focus photons in a defined energy band. The formula that gives the energy band focused by each ring is given by [8]:

$$\Delta E_i = f\frac{hc}{d}\frac{\Delta R}{R_i^2} \tag{2}$$

where ΔE_i is the energy band focused by the ith ring, f is the focal length, h is the Planck constant, c is the speed of light, R_i is the radius (at the center of the crystal) corresponding to the i-th ring, d is the crystal spacing (1.998 Ångstrom for GaAs) and ΔR is the length of the crystal along the Laue lens radius (in our case 3 cm). The first (i.e. innermost) ring is placed at R=20,7 cm and thus it focuses energies between 558–645 keV. The second ring is placed at R=23.7 cm and thus focuses energy between 492 and 558 keV and so on till the fourty-fifth and final ring which is placed at R=152.7 cm and focuses energy between 80 and 82 keV.

Thanks to the focusing effect along one direction of each crystal, the 30 mm × 10 mm dimension produces a diffracted image that is of the order of 1 × 10 mm. Indeed, the 10 mm dimension does not have any focusing effect but instead is extremely effective in the 30 mm direction. Given that in this paper we are not interested in the study of the lens response, we have not considered aberrations and/or distortions due to crystal misalignment errors. Hence, for the simulations, we have defined crystals directly as their image on to the focal plane (i.e. 1 × 10 mm^2 rectangles).

For our simulations, the equivalent dimension of each rectangle is that of the PSF (at 20 m from the lens) of a single crystal, whose real dimension is given in Table 1 [8]. These rectangles can then be arranged on concentric rings that have the same radius on the Laue lens as the real ones (Fig. 2). Photons with a random energy between E_{min} and E_{max} are then emitted from a random point inside each rectangle, and in the direction of the focal plane detector placed 20 m away from the ring. The overall PSF of the lens, for the 20 m focal length, is shown in Fig. 9, where the expected PSF of a lens made of GaAs (2 2 0) crystals is compared with the PSFs convolved with the detector response.

2.2. Focal plane detector modeling

The focal plane detector is modeled by assuming a rectangular prism structure placed at 20 m away from the modeled Laue lens. In reality, the focal plane detector will be formed of multiple layers

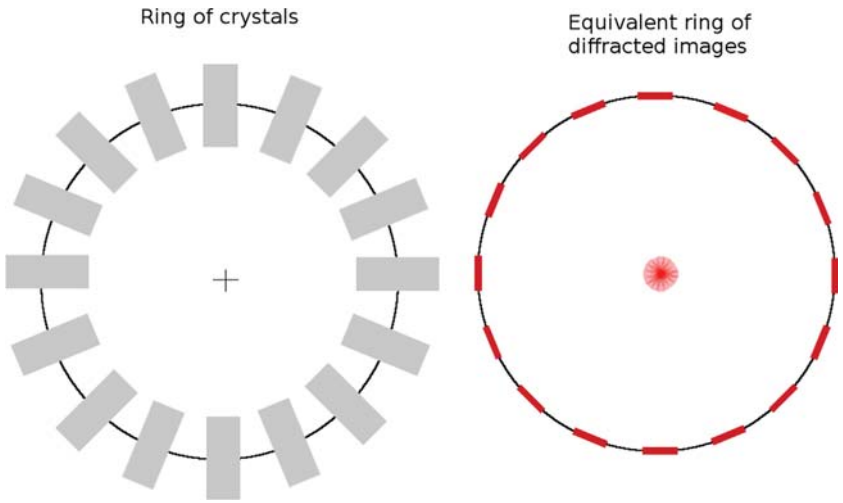

Fig. 2. *Left*: the real distribution of the crystal tiles in one of the Lens circle. *Right*: the illustration of the equivalent simulated ring.

of DSSDs because of the limitations on the sizes of silicon and germanium detectors industrially available. Then, the holding mechanical structure and the readout electronics are expected to be mounted on the sides of the detector and not in between the layers. Therefore they should not have a significant effect on the photon interaction history; the detection efficiency is not expected to be significantly degraded from the 'nominal density case' adopted in our simulations. In addition, the focal plane detector shall be placed inside an Aluminum container of a finite thickness for cooling and electrical shielding purposes. Assuming an entrance window with a very conservative thickness of 5 mm, we expect a decrease of the impinging flux by less than 3% at 100 keV and less than 1.5% at 600 keV. This evaluation includes both the photon loss by photoelectric absorption and by scattering on the passive material.

The detector is energy and 3D position sensitive. One of the objectives of this work is to optimize the position resolution in the first two dimensions. No optimization is performed on the third dimension (the depth). However, the 3D positioning capability of the detector is used in the simulation in order to reconstruct the photon interaction sequence.

3. Detection efficiency

The objective of the first set of simulations is to optimize the volume of the focal plane detector to achieve an efficiency of at least 80% at an energy in the 558–645 keV band. The simulation was performed for the innermost ring of the Laue lens defined in Table 1, using a sample of 100,000 *interacting* photons of energies from 558 keV to 645 keV with uniform distribution. Note that this sample includes 100,000 *interacting* photons; the term '*interacting*' signifies that the source of simulated lens ring keeps generating photons until 100,000 interact at least once in the focal plane detector. The number of *generated* photons, in order to get the desired number of interacting photons, is more than 100,000. The number of *generated* photons is the number of *interacting* photons plus the number of photons which undergo no interactions at all.

Two main simulations were made, one for a high density material (Germanium) and another for a low density material (Silicon). These materials were considered due to their good spectral performances, which is an essential requirement especially for the detection of the 511 keV line, and for their good achievable polarimetric performance in the energy band of the lens. The results are shown in Table 2 for a Germanium based detector and in Table 3 for a silicon based detector.

In these tables the size of the detector is varied in the three dimensions (x–y–z). For each interacting photon, the number of interactions (INT) is recorded. This is done up to 8 interactions per photon (INT = 8). In addition, photons which interact more than 8 times are recorded under one column (INT > 8). These types of events INT > 8 are not counted as good events because the computational time for their reconstruction is too large, and it would require testing of at least 9! sequences in the "Classical Compton Scattering Reconstruction (CSR)" used by the REVAN component of MEGALIB [9]. The "Bad CSR" column includes the number of photons which cannot by reconstructed by the Classical CSR used by REVAN; these only include events with INT < 9. ε is the simulated efficiency and is detailed in the following section.

3.1. Detection efficiency estimation

To estimate the efficiency ε of the detector we consider the following approach depending on the number of interactions per photon:

- INT = 1: The detector records one interaction per photon; in Tables 2 and 3, these are listed under row "INT = 1". In this case, if the photon interacts via the photoelectric effect, then the event is considered as a count. The considered ring of the LAUE lens focuses rays between 550–650 keV. Photons which deposit more than 550 keV are considered as Photoelectric events and thus as counts. These photons could not have interacted via Compton scattering because the maximum energy which can be deposited by a 650 keV photon via Compton scattering (Eq. (3)) is $\sim$46 keV < 550 keV (i.e. the case of backscattering):

$$E_{\text{dep}} = E_i - E_f = E_i - \frac{E_i}{1 + \frac{E_i}{m_e c^2}(1 - \cos\theta)} \tag{3}$$

where E_{dep} is the deposited energy, E_i is the initial photon energy, E_f is the final photon energy, $m_e c^2$ is the electron rest mass energy and θ is the Compton scattering angle. The number of photons which interact once in the detector and deposit more than 550 keV are shown in Tables 2 and 3 under the column INT = 1 and designated by the letter "p" which refers to photoelectric effect. For example, consider in Table 2 the detector of size ($2 \times 2 \times 2$ cm^3). For this detector, the total

Table 2
Optimizing the size of a Germanium-based focal plane detector.

x–y–z (cm^3)		2–2–2	5–5–5	10–10–10	10–10–12.5	15–15–15
INT=1	Total	49,393	23,106	8,673	7,694	5,875
	P	1,148	1,265	1,326	1,319	1,307
INT=2	Total	28,038	24,257	16,064	15,286	12,985
	C–P	4,028	6,014	7391	7,606	6,919
	C–C–E and > 550 keV	615	687	263	165	81
INT=3		13,171	20,965	21,286	21,289	19,877
INT=4		5,727	15,814	21,782	22,162	22,359
INT=5		2,113	9,190	16,334	16,645	18,234
INT=6		638	4,296	9,206	9,733	11,372
INT=7		140	1,489	4,270	4,499	5,588
INT=8		30	424	1,617	1,816	2,428
INT > 8		6	116	690	832	1,264
Bad CSR		5,381	5,287	5,612	5,041	5,023
No INT		86,905	16,964	2,177	810	304
ε		12%	47%	76%	80%	83%
ε'		< 0.1%	< 0.1%	< 0.1%	< 0.1%	< 0.1%

Table 3
Optimizing the size of a Silicon-based focal plane detector.

x–y–z (cm^3)		10–10–10	20–20–10	20–20–20	30–30–20	30–30–30
INT=1	Total	21,606	16,895	7,508	6,106	4,030
	P	15	20	26	15	10
INT=2	Total	23,263	16,948	12,325	9,601	7,905
	C–P	192	215	246	240	242
	C–C–E and > 550 keV	0	0	0	0	0
INT=3		17,580	13,829	12,051	9,457	8,232
INT=4		11,825	11,249	10,766	9,115	8,323
INT=5		8,412	9,613	10,418	9,488	9,307
INT=6		6,071	8,363	10,352	10,398	10,482
INT=7		4,170	7,053	9,703	10,626	11,366
INT=8		2,873	5,698	8,577	10,219	11,054
INT > 8		3,791	9,917	18,176	24,878	29,279
Bad CSR			9,918	8,022	6,801	5,086
3,96-1						
No INT		18353	18,353	2,500	2491	372
ε		35%	40%	54%	53%	54%
ε'		0%	0%	0%	0%	0%

number of photons which interact once is 49,393. Of these photons, only 1,148 deposit more than 550 keV.

- INT=2: The detector records two interactions per photon; in Tables 2 and 3, these are listed under row "INT=2". In our approach, if the sum of the energy deposits in both sides is greater than 550 keV, then the photon is considered as absorbed in the second interaction. Of course, some of these events could have undergone two Compton scatterings followed by an escape. However, we will show that the number of events where the photon interacts twice leaving a total of at least 550 keV and escape the detector are negligible and therefore our approximation is adequate. The number of photons which interact twice in the detector and deposit a sum of more than 550 keV are shown in Tables 2 and 3 under the row "INT=2" and designated by "C–P" refering to Compton–Photoelectric. In addition, photons which deposit a sum of more than 550 keV and end up escaping from the detector are designated by "C–C–E" refering to Compton–Compton–Escape. For example, consider in Table 2 the detector of size ($2 \times 2 \times 2$ cm^3). For this detector, the total number of photons which interact two times is 28,038. Of these photons, only 4643 deposit more than 550 keV. In addition, of these 4643 photons 615 escape the detector and thus only $4643 - 615 = 4028$ photons were absorbed.
- INT=3, 4, 5, 6, 7 or 8: The detector records a number of interactions between 3 and 8; in Tables 2 and 3, these are listed under row "INT=i" where i is the number of interactions of the photon and i is between 3 and 8. In this case, the photon undergoes a number of Compton scattering ending in an absorption or an escape. In both cases, the first three interactions can be used to reconstruct the incoming energy. The first three interactions are either Compton–Compton–Photoelectric or Compton–Compton–Compton. Distinguishing between these two is not vital in the energy reconstruction. The photon energy can be reconstructed according to [10]:

$$E_1 = L_1 + \frac{L_2}{2} + \frac{1}{2}\left[L_2^2 + \frac{4m_e c^2 L_2}{1 - \cos\theta_2}\right]^{\frac{1}{2}} \tag{4}$$

where E_1 is the energy of the focused photon, L_1 and L_2 are the deposited energies at the first and second interaction sites, m_e is the electron rest mass, c is the speed of light in vacuum, and θ_2 is the Compton scattering angle for the second interaction (Fig. 3). Fig. 3, represents the simplest case applicable to the reconstruction method; where INT=3. In our approach, the same energy reconstruction method can be applied for events up to INT=8 given that the interaction sequence is properly reconstructed. The uncertainty on the measured energy is discussed in [10] and is a function of the energy and position resolution of the detector.

The detector efficiency ε is estimated as given in Eq. (5):

$$\varepsilon = \frac{\mathrm{INT}_1^{550\ \mathrm{keV}} + \mathrm{INT}_2^{550\ \mathrm{keV}} + \left(\sum_{i=3}^{i=8} \mathrm{INT}_i\right) - \mathrm{INT}_{\mathrm{Bad\ CSR}}}{\text{Numbers of Photon generated}} \times 100 \tag{5}$$

(new line, was too squished)

- where $\mathrm{INT}_1^{550\ \mathrm{keV}}$ is the number of photons of type INT=1 for which photons deposit at least 550 keV.
- $\mathrm{INT}_2^{550\ \mathrm{keV}}$ is the number of photons of type INT=2 for which photons deposit a sum of at least 550 keV in both interactions. These include C–P and C–C–E events, because we assume that the detector is not able to distinguish between these two types of events. The energy is reconstructed in the case of C–P but is not in the case of C–C–E. However, the contribution of C–C–E to the total efficiency will be shown to be less than 0.1% in all cases. The contribution of events of type $\mathrm{INT}_2^{550\ \mathrm{keV}}$ Compton–Compton–Escape to the total detection efficiency is designated by ε' and reported in Tables 2 and 3.
- $\sum_{i=3}^{i=8} \mathrm{INT}_i$ is the sum of all photons of types INT=3, 4, 5, 6, 7 or 8.

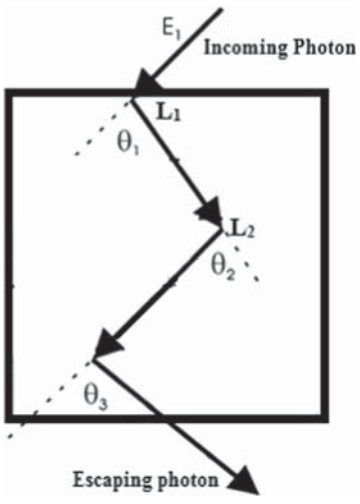

Fig. 3. A photon undergoing three interactions before escaping from the detector.

- $INT_{Bad\ CSR}$ is the number of photons of type INT = 2,3,4,5,6,7,8 whose interaction sequences cannot be reconstructed by the "Classic Compton Sequence Reconstruction" [11] method used by REVAN (Real Event Analyzer) component of the MEGALIB software library.

3.2. Germanium focal plane

In a thick Germanium DSSD, the determination of the depth of interaction (z location) for a gamma-ray interaction event can be made using the time difference in the electrons arrival at the anode and the holes arrival at the cathode [12]. Using such technique, the achievable depth resolution directly depends on the method used for the timing measurement and on its precision. In the literature, depth resolutions better that 0.5 mm are reported for different Ge DSSD configurations [12,13]. Therefore, this value can be assumed in our simulations as a reference for the achievable depth resolution in the Ge DSSD configurations considered in this work. In addition the resolution in the first two dimensions is assumed to be 500 μm which is the minimum requirement to reconstruct the point spread function of the LAUE lens (see Section 4).

Considering the results in Table 2, then for a Germanium based focal plane detector a high detection efficiency (80%) is achieved at sizes of $10 \times 10 \times 12.5\ cm^3$ or larger.

Germanium DSSDs are detectors able to measure the energy and position of an interaction. They are currently available with thicknesses up to 2 cm [14]. Therefore, the required thickness to realize high detection efficiency can be achieved by using a stack of a small number of thick Germanium DSSDs. Consequently, the total number of readout channels can be maintained limited, with a clear advantage in terms of required resources for satellite instruments. The exact number of channels depends on the required spatial resolution of these detectors and on their overall dimensions: a readout channel number of ~6500 is required for the largest ($15 \times 15\ cm^2$), thickest (15 cm) and highest spatial resolution (350 μm, see Section 4) case considered in Table 2.

3.3. Silicon focal plane

Silicon DSSDs are currently available with thicknesses up to 2 mm (see for example [15]) Therefore, to achieve the required detection efficiency hundreds of Silicon DSSDs closely arranged in a tower configuration are needed. The number of readout channels is then of the order of several tens of thousands and is still not unusual for space telescopes. For Silicon, the DSSDs locate the position of the interaction in the first two dimensions. The assumed position resolution in the first dimension is 500 μm (see Section 4). The third dimension is inherited from the DSSDs placement in a tower configuration. Then, the depth resolution of detector is the thickness of a single DSSD (i.e. 2 mm).

In Silicon both the atomic number ($Z = 14$) and density (2.65 g/cm^3) are low compared to Germanium (32, and 5.3 g/cm^3, respectively). Thus more Silicon mass is required to maintain a high detection efficiency. However, the low atomic number of Silicon increases the Compton scattering probability in the same energy band and possibly the percentage of the reconstructable photon escapes increases.

From Table 3, we see that to highest detection efficiency (~54%) is achieved at a Silicon detector size of $20 \times 20 \times 20\ cm^3$. There is no efficiency improvement when increasing the detector size to $30 \times 30 \times 20\ cm^3$ or even to $30 \times 30 \times 30\ cm^3$. The reason appears to be that when the Silicon detector size increases, the number of INT > 8 events increases equivalently to the increase in the number of accepted events (INT = 1, 2, 3, 4, 5, 6, 7 and 8). Hence the detection efficiency for a size greater than $20 \times 20 \times 20\ cm^3$ is maintained at a constant percentage of 53–54%.

3.4. Discussion

3.4.1. Germanium versus silicon: Detector efficiency

The high number of required Silicon DSSDs can be a limiting factor. In addition, these detectors have been massively produced for particle and nuclear physics experiments where the thicknesses of the wafers are typically 500 μm or less. Producing thousands of thick detectors (2000 μm) could be a problem. However, the major drawback of using Silicon DSSDs is the limitation on the detection efficiency (54%). This limitation is due to the large portion of photons which interact more than 8 times and are not sequenced. Thus we conclude that a high Z material is unavoidable to achieve high detection efficiencies.

There is no doubt that Germanium is the best gamma ray spectrometer. On the other hand Germanium's relatively higher atomic number increases the internal background. Besides the system complexity of an active cooling system in space, one has to consider the gamma ray absorption of the cryostat and the internal background increase due to the dead mass of the cryostat, the cold plates and the cryo-coolers. The impact of the cryo-coolers on the power budget can also be significant. Moreover, Germanium would require periodic annealing cycles in space to maintain its spectral performance.

A possible way out is to use Cadmium Telluride (CdTe) based detectors. CdTe has a density of 5.85 g/cm³, and a high atomic number ($Z = 48–52$) hence the required volume of CdTe would be comparable to that of Germanium. The optimization of the size of a CdTe focal plane detector is shown in Table 4. Another requirement of the detector is its ability to perform polarimetry all over its pass band. In fact, high Z materials such as CdTe are effective for polarimetry measurements only above 100–150 keV, where their Compton scattering cross-section become non-negligible. However this problem may be solved by adding a few silicon layers on top of the CdTe detector. Such a design is currently under study [16]. In addition, it should be noted that for CdTe detectors the contribution of events INT = 1 and INT = 2 is significantly large (of the order of 26%). For the remainder of this paper we will limit the discussion to comparing a high density (Ge) and a low density (Si) material.

3.4.2. Germanium versus silicon: Detector background

The main objective of this work is optimizing the efficiency and the 2D spatial resolution of a 3D focal plane spectrometer, for wide

Table 4
Optimizing the size of a CdTe-based focal plane detector.

x–y–z (cm^3)		5–5–5	10–10–5	10–10–7.5	10–10–10
INT = 1	Total	**17,962**	**15,241**	**10,838**	**8,847**
	P	**5,187**	**5,343**	**5,373**	**5,225**
INT = 2	Total	**28,134**	**26,538**	**25,364**	**25,061**
	C–P	**19,398**	**20,458**	**21,192**	**21,711**
	C–C–E and > 550 keV	**433**	**201**	**0**	**0**
INT = 3		**27,495**	**27,953**	**29,270**	**29,832**
INT = 4		**16,637**	**18,481**	**20,382**	**21,200**
INT = 5		**6,862**	**8,093**	**9,589**	**10,094**
INT = 6		**2,083**	**2,619**	**3,324**	**3,658**
INT = 7		**494**	**660**	**910**	**959**
INT = 8		**94**	**145**	**181**	**248**
INT > 8		**9**	**25**	**43**	**280**
Bad CSR		**6,252**	**5,576**	**5,652**	**5,398**
No INT		**11,940**	**11,643**	**3,587**	**1,074**
ε		**65%**	**70%**	**82%**	**87%**
ε'		**< 0.1%**	**< 0.1%**	**0%**	**0%**

Table 5
Background measured by the SPI instrument on board the INTEGRAL satellite at 100 keV and 600 keV at a High Earth Orbit (HEO), and the extrapolation of these measurements to a Low Earth Orbit (LEO, 30° Inclination and 550 km altitude). See text for details on the extrapolation.

SPI	HEO Germanium detector	Extrapolation to LEO
100 keV	6×10^{-4} c/s/keV/cm^3	3×10^{-4} c/s/keV/cm^3
600 keV	2.5×10^{-5} c/s/keV/cm^3	1.25×10^{-5} c/s/keV/cm^3

Table 6
Estimation of the background in Silicon at Low Earth Orbit.

PIN/Suzaku	Total efficiency	LEO
70 keV (measured)	0.114	$2.5 \times 10^{--5}$ c/s/keV/cm^3
100 keV	0.082	1.8×10^{-5} c/s/keV/cm^3
600 keV	0.037	1.0×10^{-5} c/s/keV/cm^3

band Laue lens. However, we have to make some consideration about the expected background level for the two types of detector materials under consideration.

A possible estimation of the background (Table 5) in a Germanium based focal plane detector can be performed using the background measured by the SPI instrument [17] on board of the INTEGRAL satellite positioned in a High Earth Orbit.

A 30° inclination and 550 km altitude LEO is taken as reference because it is the orbit of the Suzaku satellite that we will use later for the Silicon detector and also because it could represent an operational scenario also for a broad band Laue lens telescope. The instrumental background is strictly related to the rigidity cut-off R_c (GV) due to the geomagnetic field in the operational orbit. Therefore, a rough evaluation of the instrumental background level in a particular orbit (i.e. LEO with 30° inclination and 550 km altitude) with respect to a measurement in a different one (HEO for the SPI/INTEGRAL) can be evaluated by [18]:

$$B^{\mathrm{LEO}}(E) = B^{\mathrm{HEO}}_{\mathrm{SPI}}(E) \times \frac{M(9.6\ \ \mathrm{GV})}{M(2\ \ \mathrm{GV})} \approx B^{\mathrm{HEO}}_{\mathrm{SPI}}(E) \times \frac{0.66}{1.33} \approx 0.5 \times B^{\mathrm{HEO}}(E) \quad (6)$$

where $M(R_c)$ is the empirical rigidity factor [18]. The values 9.6 GV and 2 GV are the rigidity cut-offs evaluated respectively for the assumed LAUE telescope LEO and INTEGRAL/SPI HEO.

For the Silicon focal plane detector we can start from the background data measured at LEO (30° inclination, 550 km altitude) by the PIN detector of the Suzaku satellite [19]. The PIN detector is a subsystem of the hard X-ray instrument of this satellite and is made by an array of PIN Si diode (2 mm thick) and with an overall sensitive area of 160 cm^2 and operative up to 80 keV.

To extrapolate the background count rate per unit volume from that measured at 70 keV, we have evaluated the detection efficiency of the 2 mm thick Silicon at three energies (70, 100 and 600 keV). Then we multiplied the value at 70 keV by the ratio between the respective efficiencies. The inferred values are reported in Table 6. Of course this approach can be considered consistent with photon induced background, but less for charged particle induced background, because of the different absorption mechanisms (e.g. bremsstrahlung).

In fact, what has been observed by Suzaku and also foreseen by simulations for the LAD detector on LOFT [20], is that the background tends to become quite flat over a threshold (where the diffuse cosmic X-ray back ground become negligible with respect to the instrument background). Therefore, the values reported in Table 6 can be used, at least, to make a draft comparison between the two focal plane detector configurations (Germanium and Silicon).

The comparison between the values reported in Table 5 (Germanium DSSD) and the ones in Table 6 (Silicon DSSD) show that the expected background in the two extremes of the Laue operating band is lower for the Silicon based focal plane with respect to the Ge focal plane. In fact, the difference is effective at low energy (at 100 keV, Ge background is ~17 times worse), but is almost negligible at high energy (600 keV) where Ge background is only ~1.25 times the Si expected background. Of course, this disadvantage is partially recovered because Germanium is more efficient than Silicon and therefore with the same thickness the Ge focal plane provides better signal reception from the source.

Note that in scaling the HEO measured background (i.e. SPIE/INTEGRAL) to LEO we have not considered the fraction due to activation, and therefore our estimate is conservative. Furthermore, our present background evaluation has not taken into account the possibility of significantly reducing the background and the difference between the two types of focal plane detectors using their high 3D segmentation. As previously highlighted, the 3D spatial resolution will allow a reliable reconstruction of the incoming direction of the impinging photons. Therefore, in the proposed Laue telescope operating energy band, we can expect an effective background at least equal or better than the one measured by Phoswich detectors of the SAX/PDS instrument [21,22].

4. Point spread function reconstruction

The objective of this simulation is to optimize the two dimensional position resolution of the focal plane detector to reconstruct the Point Spread Function (PSF). For simplicity, only on-axis sources have been considered. In this case, the main factor which affects the shape of the PSF is the penetration power of the photons. In this discussion we will define three types of PSF:

- The Ideal PSF: where the photon deposits all of its energy on the surface of the focal plane detector (i.e. there is no penetration inside the detector depth and no multiple interactions for a single photon).
- The total PSF: where all the interaction points of the photons are taken into account in the PSF (i.e. if a single photon undergoes more than one interaction, all of these interactions are taken into account in the PSF). In this case, the PSF is distorted from the ideal case due to accounting for multiple interaction points per single photon.
- The Reconstructed PSF: where the three dimensional capability of the focal plane detector is utilized to reconstruct, using Compton Kinematics, the first interaction position. In this case, distortions due to multiple interactions per single photon are omitted. However, since the first interaction point is not necessarily at the surface of the detector, there are slight distortions from the ideal PSF.

For illustration purposes, a comparison between a total, ideal and reconstructed PSF is given in Fig. 4.

The main concern is for the inner rings of the lens. These rings are the ones which focus the photons with highest energies in the lens pass band. And thus, these photons are those that most likely penetrate inside the detector and interact multiple times causing more distortions in the PSF shape. According to the study in [8], we evaluated the PSF half power width (HPW), i.e. the radius of the circle that contains 50% of the incoming source photons. We will use this fact as a guide to optimize the position resolution of the detector. The minimum requirement is that the resolution

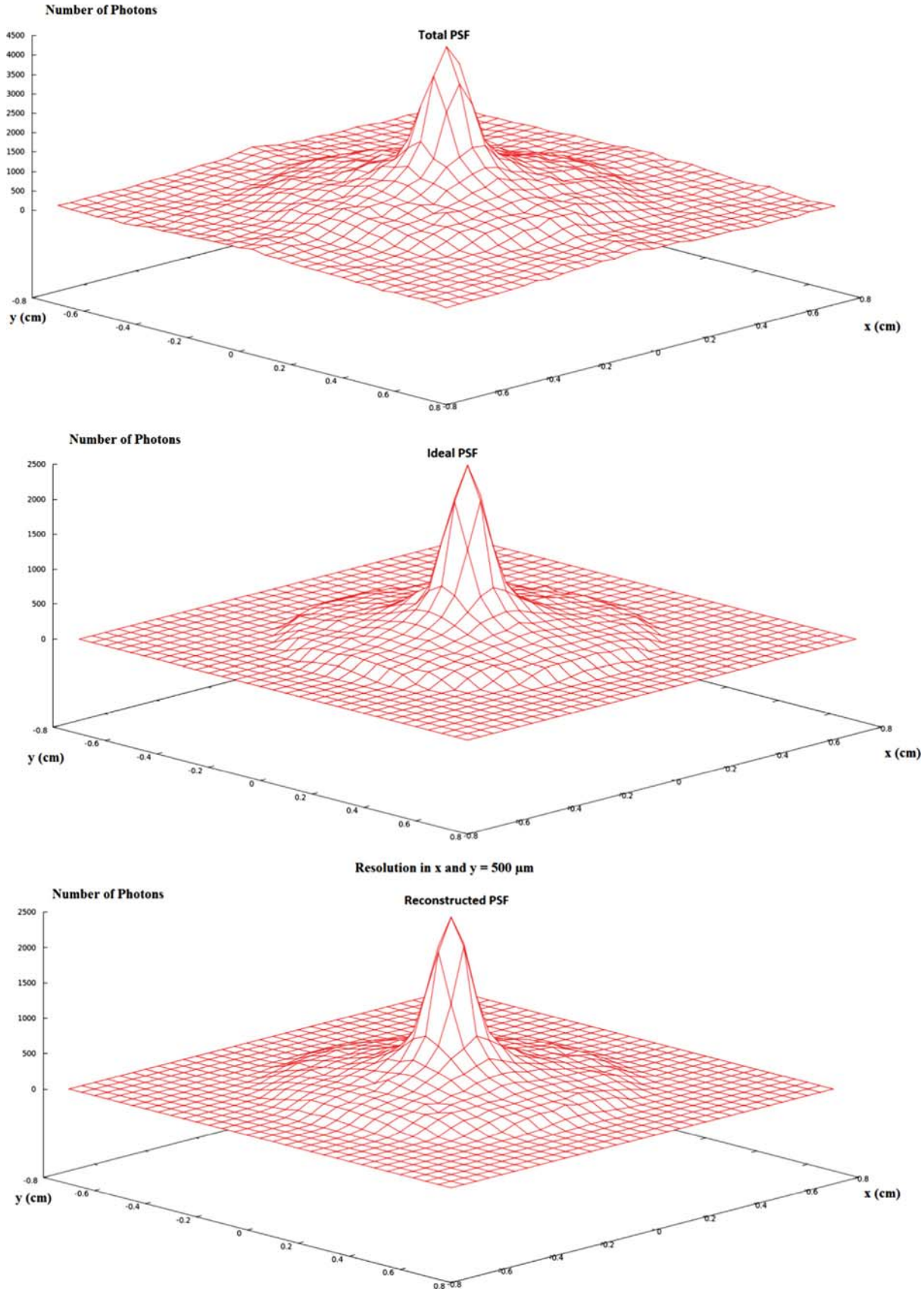

Fig. 4. Comparing the total, ideal and reconstructed PSF for a sample of 100,000 interacting photons focused on a germanium focal plane detector.

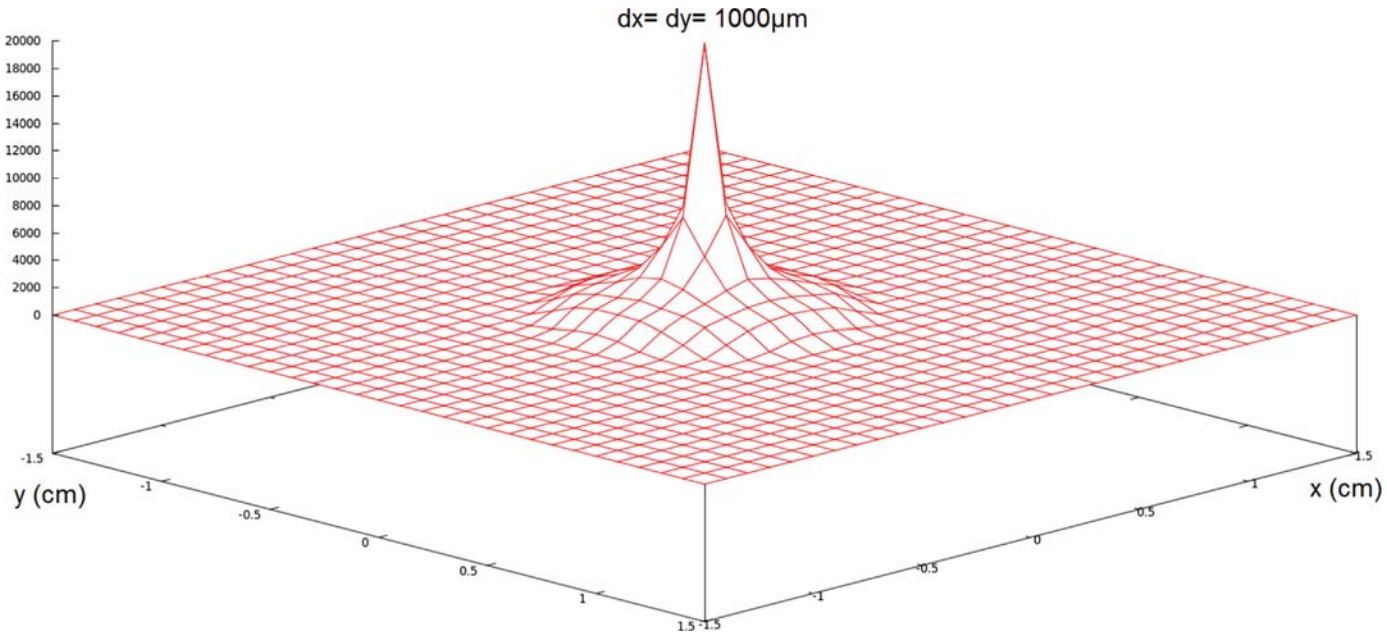

Fig. 5. Reconstructed PSF in Germanium for ring-1 for a sample of 250,000 interacting photons. Resolution on the x and y axes is 1000 μm.

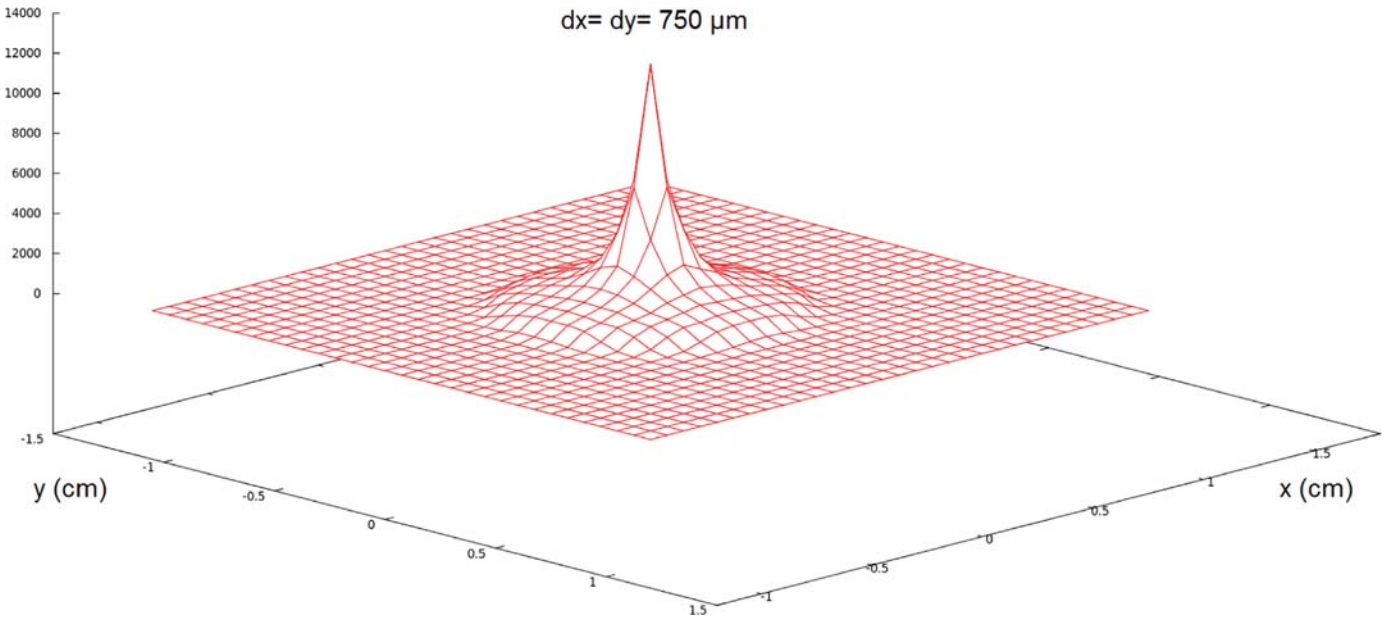

Fig. 6. Reconstructed PSF in Germanium for ring-1 for a sample of 250,000 interacting photons. Resolution on the x and y axes is 750 μm.

must be good enough so that these 50% photons are read on at least three strips, i.e. on three detector equivalent pixels.

First we will present the case for optimizing the two dimensional position resolutions using reconstructed PSF, and then we will present a comparison between the ideal PSF, the total PSF and the reconstructed PSF. The PSF simulations will first be detailed for the Germanium detector case. Then a comparison will be made with simulations in the Silicon detector case.

4.1. High energy PSF simulation in germanium

The following simulations have been performed for ring-1 of the Lens, i.e. $\Delta E = 558–645$ keV, assuming a Germanium detector. Four different spatial resolutions in the (x, y) plane were considered: $dx = dy = 1000$ μm, 750 μm, 500 μm, 350 μm. The number of simulated photon interactions is 250,000 with uniform energy distribution between 558 and 645 keV. The accepted events in the PSF are those where the photon:

- Interacts once and deposits at least 550 keV.
- Interacts twice while depositing a total of 550 keV or more.
- Interacts more than 2 times but less than 9 times.
- Can be reconstructed by the Classic Compton Sequence Reconstruction algorithms used by REVAN.

For these accepted events, only the position of the first interaction position is accounted for in order to evaluate the reconstructed PSF. The reconstructed PSF for each spatial resolution is shown in Figs. 5–8.

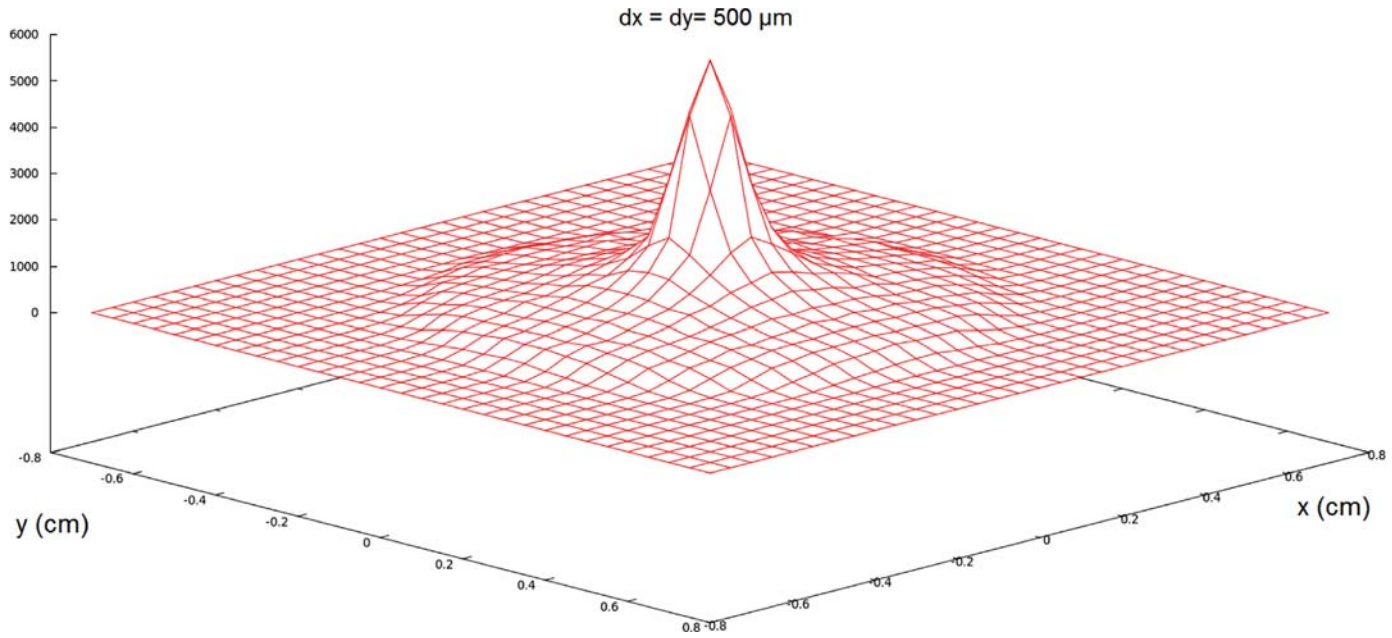

Fig. 7. Reconstructed PSF in germanium for ring-1 for a sample of 250,000 interacting photons. Resolution on the x and y axes is 500 μm.

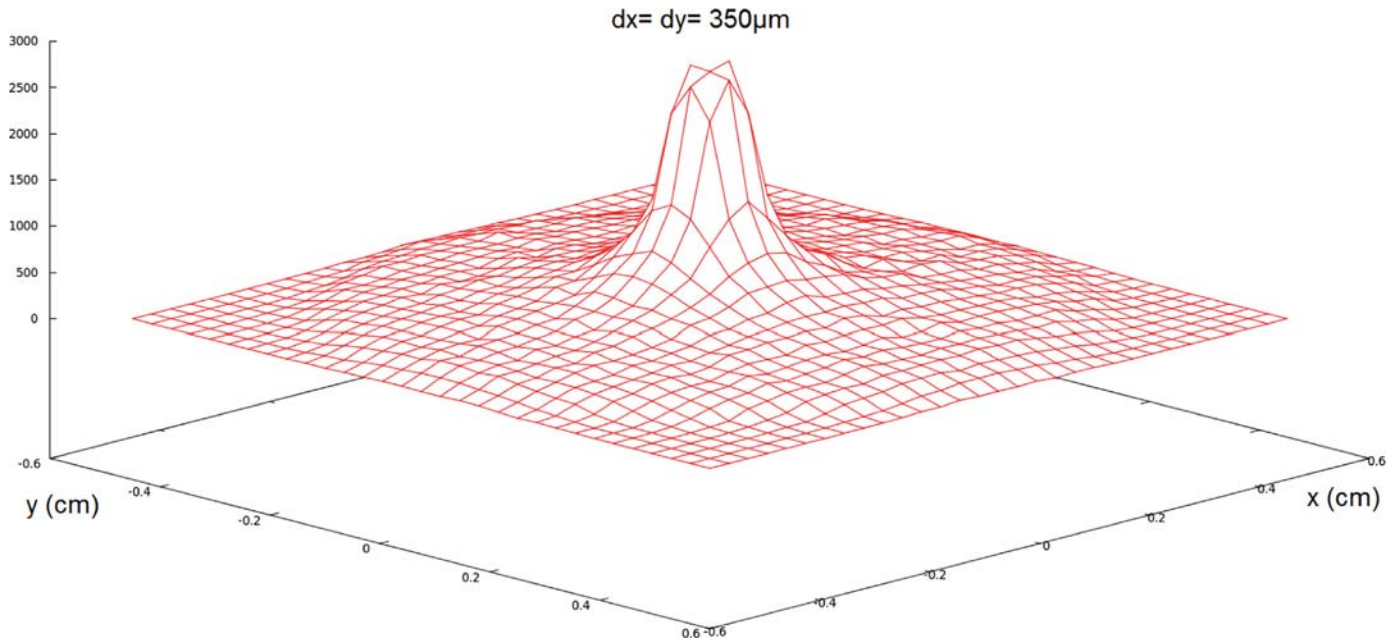

Fig. 8. Reconstructed PSF in germanium for ring-1 for a sample of 250,000 interacting photons. Resolution on the x and y axes is 350 μm.

In order to evaluate the HPW of each simulated distribution, we will take a 2D slice from each of the three dimensional PSFs above. The slice is done at $y=0$. The slices extracted from each PSF are plotted in Fig. 9 and normalized to their respective total number of accepted counts.

The total number of detected photons in the 2D slice corresponding to dx = 1000 μm is 51,311. Of these photons, 39% are found in the central strip, while 15% of these photons are found respectively in each of the first neighbor pixels. This adds up to 69% on the three central strips. So a spatial resolution of 1000 μm is too low, failing to reconstruct the PSF under the initially set objectives. In the case of $dx=750$ μm, the three central pixels contain 62% of the detected photons that represent an improvement of 7% but still fail to meet our requirements. Considering a resolution of 500 μm, the PSF is reconstructed with the three central strips containing 51% of the detected photons. Therefore a spatial resolution of 500 μm appears to provide a good enough sampling of the PSF and we can set it as a minimum requirement. In the last simulated case corresponding to 350 μm spatial resolution, the three central pixels contain 13%, 13% and 13% of the detected photons, respectively. This means that we need more than three (at least five) spatial bins to have 50% of the PSF counts. In this case, the reconstruction of the PSF can be obtained with great precision, and this spatial resolution value can be adopted as a desirable target for the design of the focal plane detector.

Fig. 10 shows a comparison between the 2D slices of the 3D ideal, total and reconstructed PSFs. By sequencing the photon interaction history it is possible to significantly reduce the distortion in the PSF and get very close to the ideal PSF case.

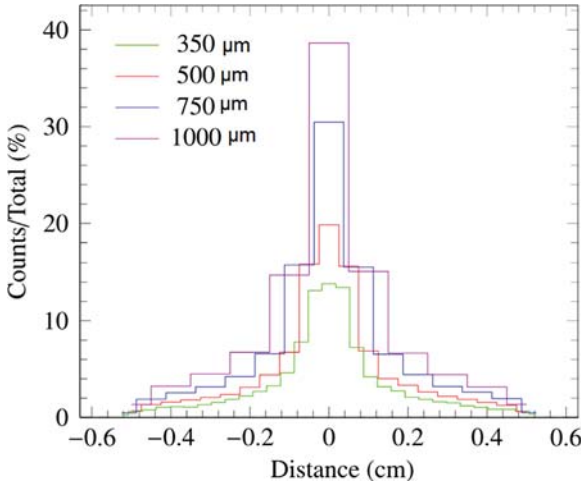

Fig. 9. One row slice (at $y=0$) for the Reconstructed PSF. Each curve is normalized to its respective total accepted events.

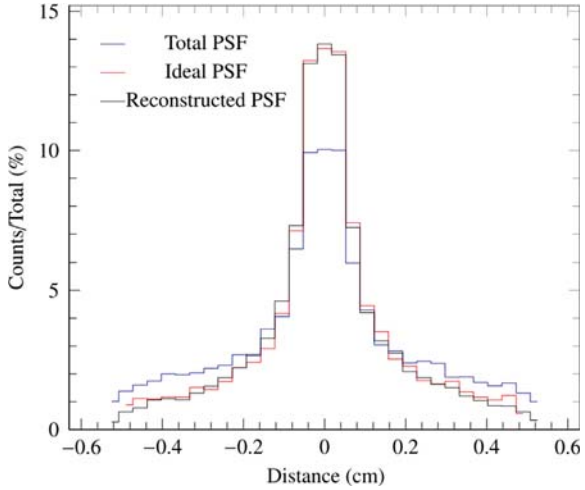

Fig. 10. PSF comparison for 350 μm spatial resolution on the x and y axes.

4.2. Comparing the reconstructed PSF of a different material

The PSF reconstruction simulation made for Germanium was then made for Silicon. The number of impinging photons is 250,000. We have assumed the same set of spatial resolution in the (x, y) plane used for the Ge case: 1000, 750, 500 and 350 μm. In addition we considered the same criteria of accepted event selection in the PSF reconstruction. The percentage of photons detected in the central 7 pixel was recorded and summarized in Table 7. The following conclusions can be derived from this table:

- Changing the material has negligible effects on the spread of the PSF over the strips for all of the considered position resolutions.
- For a position resolution of 500 μm the three central strips contain a similar number of detected photons in both Germanium and Silicon; 51% for both materials.

In conclusion we set 500 μm as a minimum requirement for the focal plane spatial resolution; i.e. the pitch of the detector. Using this information, the capacitance of these DSSDs can be simulated; this is discussed in the following section.

5. Response simulations of the double sided strip detectors with SILVACO

One of the major contributions to the noise of the DSSD comes from the capacitive coupling between the DSSD strips. There are two types of capacitance that originate from this coupling. The first is the interstrip capacitance which is the coupling between a strip and all of the other strips on the same side. The second is the bulk capacitance which is the coupling between a strip and all of the other strips on the opposite side. The bulk capacitance can also be used to estimate the full depletion voltage of DSSDs. By increasing the voltage, the capacitance decreases exponentially until reaching the limit at full depletion conditions.

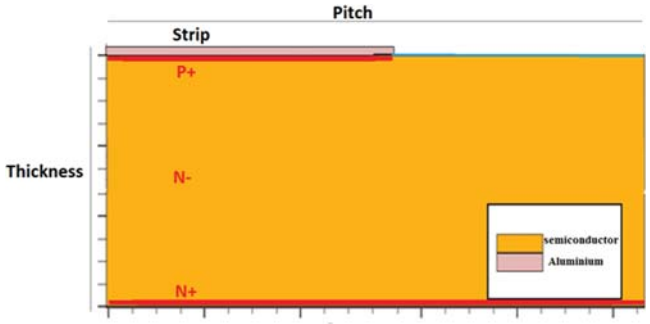

Fig. 11. A single cell of a DSSD in SILVACO.

Table 7
Percentage of photons read in the central 7 strips of the focal plane detector. Two materials are considered: Germanium and Silicon. The detector pixel resolution is varied between 350, 500, 750 and 1000 μm.

Material	x–y Resolution (μm)	Third neighbor left (%)	Second neighbor left (%)	First neighbor left (%)	Central strip (%)	First neighbor right (%)	Second neighbor right (%)	Third Neighbor right (%)
Germanium	350	4	7	13	14	13	7	4
	500	4	7	16	19	16	7	4
	750	4	7	16	31	16	7	4
	1000	4	7	15	39	15	7	4
Silicon	350	4	7	13%	14	13	7	5
	500	4	7	15	20	16	7	4
	750	4	7	16	30	16	7	4
	1000	4	7	15	39	15	7	4

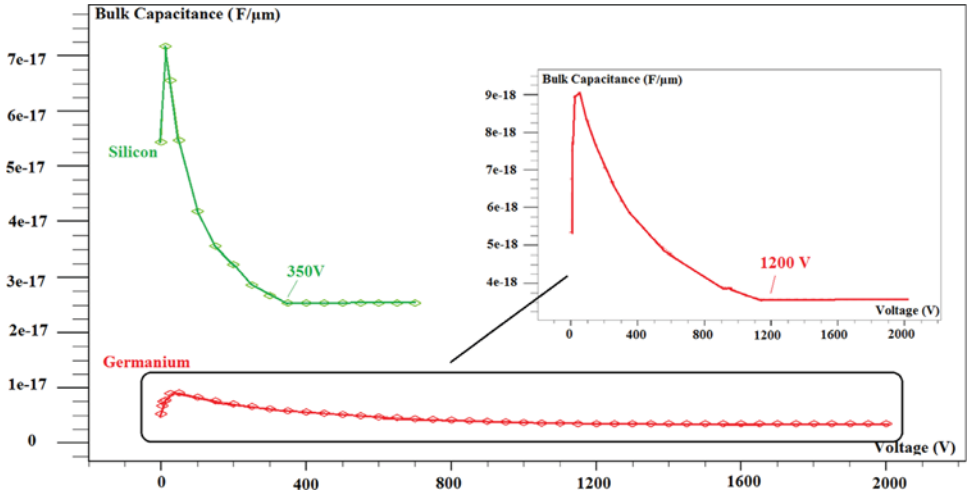

Fig. 12. The simulated bulk capacitance versus the biasing voltage for the silicon and germanium DSSDs.

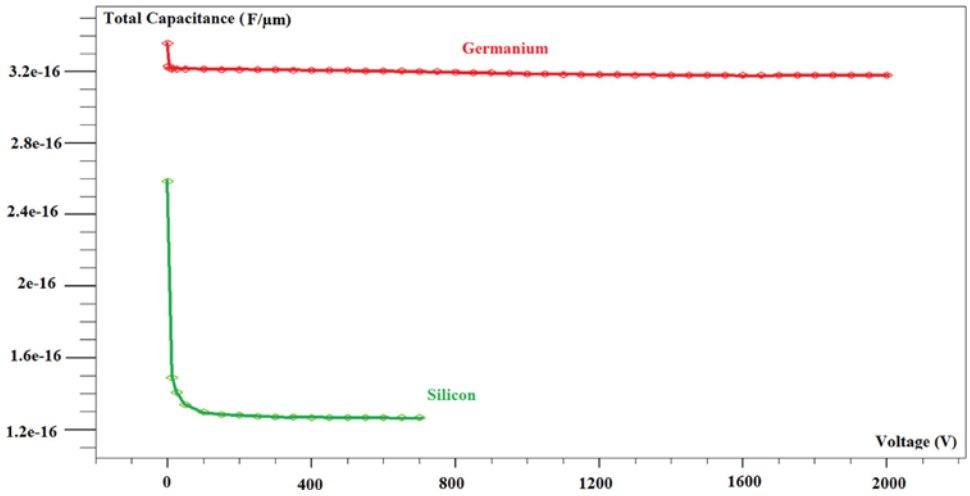

Fig. 13. The simulated total capacitance of the silicon and germanium DSSDs.

5.1. *DSSD structure in SILVACO*

Using the DEVEDIT component of SILVACO a two dimensional structure for the DSSD was created (Fig. 11). For Silicon and Germanium, the bulk of the DSSD is a weakly Arsenic doped n wafer. The p strips and n strips are heavily doped wafers with Boron and Arsenic, respectively. The capacitance of the DSSD is governed by its thickness, pitch and strip size. For simplicity the strip size was defined as a fraction of the pitch itself. The pitch gives the geometrical spatial resolution of the DSSD and it was set at 500 μm. The thickness is needed to be the largest possible to reduce the number of required DSSDs to achieve a high detection efficiency. Hence the thickness is set to 2 mm for the Silicon wafer and to 20 mm for the Germanium wafer. The strip/pitch ratio was set to 0.3. This value is a good compromise between the need to limit both the capacitance (which is lower for lower ratios) and the dead volume (i.e. low electric field zones) between the electrodes (which may increase for very low ratios).

5.2. *Capacitance simulations and results*

Using the ATLAS component of SILVACO, a positive potential is applied to the n side of the DSSD while grounding the strips on the p side. The simulated bulk capacitance versus the reverse biasing voltage is plotted in Fig. 12. Consider the plot for the silicon DSSD, the bulk capacitance starts at 7.1×10^{-17} F/μm and decreases exponentially with the increase of the voltage. At 350 V, the capacitance reaches its limiting value at about 2.5×10^{-17} F/μm suggesting that full depletion occurs at this bias. Similarly, the germanium DSSD is fully depleted at about 1200 V with a bulk capacitance of 3.5×10^{-18} F/μm.

The total capacitance was then simulated for each detector and the results are plotted in Fig. 13. The total capacitance in the full depletion (i.e. maximum sensitive volume) condition is then:

- 1.3×10^{-16} F/μm at 350 V for the silicon DSSD
- 3.2×10^{-16} F/μm at 1200 V for the germanium DSSD

6. Conclusion

We have performed a first simulation study of a focal plane detector for the LAUE project. The considered detector is made of double sided strip detectors able to measure the energy and position of a photon interaction within its volume. Two materials were compared: Germanium and Silicon. An optimization of the required detector volume to achieve at least 80% efficiency at 550–650 keV was made. This energy range corresponds to the upper

limit of the pass band of the lens considered in the LAUE project. Then, an optimization of the detector spatial resolution was made. A resolution of at least 500 μm in the *x* and *y* coordinates is found to be able to reconstruct the Laue lens Point Spread Function with enough precision. Finally, the SILVACO software was used for evaluating the final detector performance by simulating the capacitance per strip of double sided strip detectors.

The detection efficiency of a Silicon detector was found to be limited at 54%. Hence, we conclude that using a high density material (Germanium) appears to be unavoidable to achieve the required high detection efficiency. However the complexity of using Germanium in space under optimal conditions may be a limiting factor. For this reason we are also studying the possibility of using, as an alternative, a room temperature semiconductor such as CdTe/CZT despite its limited polarimetry abilities at low energies (< 150 keV) and lower spectroscopic performance. An improvement of the detector in achieving good polarimetric capabilities at low energies is possible by combining Silicon double sided strip detectors on top of CdTe pixel detectors. Hence, further simulations need to be made to optimize the focal plane detector configuration for polarimetry at low energies.

Acknowledgements

We acknowledge the ASI Italian Space Agency for its support to the LAUE project under contract I/068/09/0.

References

[1] F. Frontera et al., Scientific prospects in soft gamma-ray astronomy enabled by the LAUE project, in: Proceedings of the SPIE: Optics for EUV, X-Ray, and Gamma-Ray Astronomy VI, 886106, 2013, http://dx.doi.org/10.1117/12.2023589.
[2] F. Frontera, P. von ballmoos, Laue gamma ray lenses for space astrophysics status and prospects, X-Ray Optics and Instrumentation, Special Issue on X-Ray Focusing: Techniques and Applications, id. 215375, 2010.
[3] M. Khalil, Study of Strip Spectro-imaging Detectors for a Future Space MeV Telescope Ph.D. Thesis, University of Paris Diderot-France and University of Ferrara-Italy, 2014.
[4] H.F.-W Sadrozinski, et al., IEEE Transactions Nuclear Science 48 (2003) 933.
[5] D. Pellicciotta, et al.IEEE Transactions Nuclear Science 53 (2006) 253.
[6] Zoglauer, et al., New Astronomy Reviews 50 (2006) 629.
[7] ⟨http://www.silvaco.com/⟩.
[8] V. Valsan, Extending the Band of Focusing X-ray Telescopes Beyond 100 keV: Motivations and Proposed Solutions Ph.D. Thesis, University of Ferrara-Italy, 2013.
[9] Zoglauer, et al., NeWAR 50 (2006) 629.
[10] Kurfess et al., Compton Scatter Imaging Instrument, US patent 6528795 B2, (2003).
[11] Oberlack U. et al., A Compton Scattering Sequence Reconstruction Algorithm for the Liquid Xenon Gamma-ray Imaging Telescope (LXeGRIT), SPIE 4141, (2000) 168.
[12] M. Amman, P.N. Luke, Nuclear Instruments & Mehtods A 452 (2000) 155.
[13] Bandstra M.E., et al., Position calibrations and preliminary angular resolution of the prototype nuclear compton telescope, in: IEEE Nuclear Science Symposium Conference Record, 2006, p. 770.
[14] I. Mateu, et al., Proceedings of SPIE 8852 (2013) 88520Q-1.
[15] ⟨http://www.micronsemiconductor.co.uk/product.asp⟩, [Online].
[16] T. Tanaka, et al., Nuclear Instruments and Methods A 568 (2006) 375.
[17] P. Jean, et al., Astronomy & Astrophysics 411 (2003) L107.
[18] A.J. Dean, et al., Astronomy & Astrophysics 219 (1987) 358.
[19] Y. Fukazawa, et al., Publications of the Astronomical Society of the Pacific 61 (2009) S17.
[20] R. Campana, et al., Experimental Astronomy 36 (2013) 451.
[21] F. Frontera, et al., SPIE Proceedings 3114 (1997) 206.
[22] F. Frontera, et al., Astronomy & Astrophysics Supplement Series 322 (1997) 357.